Atmos. Chem. Phys. Discuss., 14, 1525–1557, 2014
www.atmos-chem-phys-discuss.net/14/1525/2014/
doi:10.5194/acpd-14-1525-2014

Atmospheric Chemistry and Physics Discussions
Open Access

Analysis of the effect of water activity on ice formation using a new thermodynamic framework

D. Barahona

Global Modeling and Assimilation Office, NASA Goddard Space Flight Center, Greenbelt, Maryland, USA

Received: 25 October 2013 – Accepted: 3 January 2014 – Published: 17 January 2014

Correspondence to: D. Barahona (donifan.o.barahona@nasa.gov)

Published by Copernicus Publications on behalf of the European Geosciences Union.

Abstract

In this work a new thermodynamic framework is developed and used to investigate the effect of water activity on the formation of ice within supercooled droplets. The new framework is based on a novel concept where the interface is assumed to be made of liquid molecules "trapped" by the solid matrix. Using this concept new expressions are developed for the critical ice germ size and the nucleation work, with explicit dependencies on temperature and water activity. However unlike previous approaches, the new model does not depend on the interfacial tension between liquid and ice. Comparison against experimental results shows that the new theory is able to reproduce the observed effect of water activity on nucleation rate and freezing temperature. It allows for the first time a phenomenological derivation of the constant shift in water activity between melting and nucleation. The new framework offers a consistent thermodynamic view of ice nucleation, simple enough to be applied in atmospheric models of cloud formation.

1 Introduction

Ice formation by freezing of supercoooled droplets is an important natural and technological process. In the atmosphere it leads to the formation of cirrus and determines the freezing level of convective clouds (Pruppacher and Klett, 1997). At temperatures below 238 K and in the absence of ice forming nuclei, freezing proceeds by homogeneous nucleation. A significant fraction of cirrus in the upper troposphere form by this mechanism (Gettelman et al., 2012; Barahona et al., 2013). Cirrus clouds impact the radiative balance of the upper troposphere (Fu, 1996) and play a role in the transport of water vapor to the lower stratosphere (e.g., Barahona and Nenes, 2011; Jensen and Pfister, 2004; Hartmann et al., 2001). Correct parameterization of ice formation is therefore crucial for reliable climate and weather prediction (Lohmann and Feichter, 2005). Many experimental and theoretical studies have been devoted to the study of

ACPD
14, 1525–1557, 2014

homogeneous nucleation (e.g., Kashchiev, 2000; Murray et al., 2010b; Wu et al., 2004, and references therein), yet there are still significant gaps in the understanding of ice formation within supercooled droplets.

Fundamental understanding of homogeneous nucleation has come from molecular dynamics (MD) simulations (e.g., Matsumoto et al., 2002; Moore and Molinero, 2011; Brukhno et al., 2008; Errington et al., 2002; Bauerecker et al., 2008). Density functional theory and direct kinetic models have also been employed (e.g., Laaksonen et al., 1995). Matsumoto et al. (2002) showed that ice nucleates when long-lived hydrogen bonds accumulate to form a compact initial nucleus. Errington et al. (2002) suggested that the formation of the initial nucleus was cooperative, that is, only occurs when molecules accrete into a large enough cluster of low density (LD) regions. The enthalpy of water molecules in such regions tends to resemble that of the liquid. It has been shown that the formation of LD regions within supercooled water is associated with an increase in the fraction of four-coordinated molecules (Moore and Molinero, 2011), and is thought to precede the formation of ice (Moore and Molinero, 2011; Brukhno et al., 2008; Bullock and Molinero, 2013).

MD and other detailed approaches offer a unique look at the microscopic mechanism of ice nucleation. However for climate simulations and other large scale applications, simplified and efficient descriptions of ice nucleation are required. Thus, in atmospheric modeling the theoretical study of homogeneous ice nucleation has been historically approached using the Classical Nucleation Theory (CNT) (e.g., Khvorostyanov and Curry, 2004; Dufour and Defay, 1963; Pruppacher and Klett, 1997), used to generate ice cloud formation parameterizations (Khvorostyanov and Curry, 2004, 2009).

CNT is often criticized due to the usage of the so-called capillary approximation, i.e., the assumption that the properties of ice clusters at nucleation are the same as those of the bulk (Kashchiev, 2000). This assumption is critical when considering the ice–liquid interfacial tension (also called specific surface energy), σ_{iw}, as CNT calculations are very sensitive to σ_{iw}. Direct measurement of σ_{iw} is typically difficult and surrounded with large uncertainty (Pruppacher and Klett, 1997; Digilov, 2004). Factors like crys-

ACPD
14, 1525–1557, 2014

tal shape, type and size, and the characteristics of the ice–liquid interface may also play a role in determining σ_{iw} (Wu et al., 2004; MacKenzie, 1997; Kashchiev, 2000; Murray et al., 2010a). To overcome these limitations, σ_{iw} is often found by fitting CNT predictions to experimental measurements of the nucleation rate (e.g., Murray et al., 2010a; Khvorostyanov and Curry, 2004; MacKenzie, 1997). However σ_{iw} obtained by this method often differs significantly from theoretical estimates (MacKenzie, 1997), casting doubt into the validity of CNT.

Due to the shortcomings of CNT, experimental correlations are most often used to describe homogeneous freezing in atmospheric models (e.g., Barahona and Nenes, 2008; Kärcher and Lohmann, 2002). Experimental studies generally agree on the freezing temperature of pure water with typical variation of the order of 1 K (which however may represent a variation of about two orders of magnitude in nucleation rate) (Murray et al., 2010a; Pruppacher and Klett, 1997; Riechers et al., 2013). For liquid solutions this picture is complicated by the chemical heterogeneity of liquid droplets in the atmosphere. Empirical correlations were often developed based on $(NH_4)_2SO_4$ and H_2SO_4 model solutions (e.g., Tabazadeh et al., 1997; Jensen et al., 1991). This issue was resolved by Koop et al. (2000) who demonstrated that when parameterized in terms of the water activity, a_w, freezing temperatures become independent of the nature of the solute. Furthermore, the authors showed that when plotted in a T–a_w diagram, the melting and nucleation curves can be translated by a constant shift in water activity. This particular behavior has been confirmed by several independent studies (e.g., Marcolli et al., 2007; Wang and Knopf, 2011; Knopf and Rigg, 2011; Alpert et al., 2011) and has been referred as the "water activity criteria". The Koop et al. (2000) (hereafter K00) parameterization has been incorporated in several global atmospheric models (e.g., Barahona et al., 2010; Liu et al., 2007; Lohmann and Kärcher, 2002).

The empirical model of Koop et al. (2000) offers no information on the mechanism of nucleation, however suggests that a general thermodynamic formulation of ice nucleation in supercooled solutions, independent of the nature of the solute, can be achieved. Yet, such theory has been elusive. Current formulations of CNT carry a de-

ACPD
14, 1525–1557, 2014

pendency on a_w and it has been suggested that CNT can explain the water activity criteria (e.g., Khvorostyanov and Curry, 2004). However in these studies σ_{iw} is typically modified to adjust CNT to K00, and the results obtained in this way are not independent of Koop et al. (2000) data. In fact, Koop et al. (2000) suggested that CNT and K00 can be reconciled if σ_{iw} is allowed to vary with a_w (also shown by Alpert et al., 2011) although no theoretical support was provided for it. Baker and Baker (2004) took an alternative approach and showed that the freezing temperatures measured by K00 were consistent with the point of maximum compressibility of water. The authors derived an empirical relation between a_w and the osmotic pressure which was then to used to determine freezing temperatures. The work of Baker and Baker (2004) demonstrated that the water activity criteria can be understood in terms of the compressibility of water as long as certain empirical criteria are met. However a theoretical basis for this behavior was not provided. Recently Bullock and Molinero (2013) assumed that low density regions in supercooled water are in equilibrium with bulk water and developed an expression for the freezing temperature of water as a function of a_w that roughly agrees with the results of Koop et al. (2000). Their parameterization however depends on the enthalpy difference between the hypothetical four-coordinated liquid and pure water, which is semi-empirically treated and found by fitting their MD results.

In this work a new theoretical approach is proposed to describe ice formation by homogeneous nucleation. The new model relies on a novel picture of the solid-liquid transition placing emphasis on the entropy changes across the interface. The new model is used to analyze the effect of water activity on ice formation and ice nucleation rate.

2 Theory

Consider the system of Fig. 1. The liquid droplet is assumed to be large enough so that nucleation is more likely to occur within the bulk of the liquid than at the droplet surface. The liquid is assumed to be homogeneously mixed and its cluster distribution in steady state. For simplicity it is assumed that only two components are present in

ACPD
14, 1525–1557, 2014

solution, water (subscript, "w") and a solute (subscript, "y"), although this assumption can be easily relaxed if more than one solute is present. The Gibbs free energy of the system in stage 1 (before the ice germ formation) is given by

$$G_1 = N_w \mu_{w,1} + N_y \mu_{y,1} \tag{1}$$

where N_w and N_y are the total number of water and solute molecules present in the liquid phase, respectively, and $\mu_{w,1}$ and $\mu_{y,1}$ their respective chemical potentials.

After the formation of the germ (stage 2, Fig. 1) it is advantageous to consider the solid–liquid interface as a phase distinct from the bulk (Gibbs, 1957). It is assumed that no atoms of y are present in the bulk of the solid phase although they may be present at the interface. However the dividing surface is selected so that the molecular excess of solute at the interface is zero (this is further analyzed in Sect. 2.1). The assumption of a solute-free solid is justified on molecular dynamics simulations showing rejection of ions into a unfrozen layer of brine away from the germ (Bauerecker et al., 2008). With this, the Gibbs free energy of the system in stage 2 is given by

$$G_2 = (N_w - n_s - n_{ls})\mu_{w,2} + N_y \mu_{y,2} + n_s \mu_{w,s} + n_{ls} \mu_{w,ls} \tag{2}$$

where n_s and n_{ls} are the number of atoms in the bulk of the germ and in the interface, respectively, and $\mu_{w,s}$ and $\mu_{w,ls}$, their chemical potentials. Equation (2) can be reorganized as,

$$G_2 = N_w \mu_{w,2} + N_y \mu_{y,2} + n_s(\mu_{w,s} - \mu_{w,2}) + n_{ls}(\mu_{w,ls} - \mu_{w,2}) \tag{3}$$

Using Eqs. (1) and (3) the work of germ formation, $\Delta G = G_2 - G_1$, can be written as

$$\Delta G = \Delta G_{sln} + n_s(\mu_{w,s} - \mu_{w,2}) + n_{ls}(\mu_{w,ls} - \mu_{w,2}) \tag{4}$$

where ΔG_{sln} is the change in the Gibbs free energy of the bulk solution caused by the appearance of the germ, i.e.,

$$\Delta G_{sln} = N_w(\mu_{w,2} - \mu_{w,1}) + N_y(\mu_{y,2} - \mu_{y,1}) \tag{5}$$

ACPD
14, 1525–1557, 2014

Equation (4) indicates that the work of germ formation originates from (i) changes in the composition of the liquid phase, (ii) the formation of the interface and (iii) the formation of the bulk of the solid. Using the equilibrium between ice and the liquid solution as reference state, the latter can be written in the form (Kashchiev, 2000),

$$\mu_{\mathrm{w,s}} - \mu_{\mathrm{w},2} = -k_{\mathrm{B}}T \ln\left(\frac{a_{\mathrm{w}}}{a_{\mathrm{w,eq}}}\right) \tag{6}$$

where k_{B} is the Boltzmann constant, $a_{\mathrm{w,eq}}$ is the equilibrium water activity between bulk liquid and ice, and a_{w} is the activity of water in stage 2.

ΔG_{sln} in Eq. (5) arises because the solute must be "unmixed" (Black, 2007) from the liquid to form a solute-free germ. This causes a change in the molar composition of the liquid phase and an entropic cost to the system (Bourne and Davey, 1976). Thus, ΔG_{sln} is proportional to the mixing entropy of the system,

$$\frac{\Delta G_{\mathrm{sln}}}{k_{\mathrm{B}}T} = -N_{\mathrm{w}} \ln\left(\frac{a_{\mathrm{w}}}{a_{\mathrm{w},1}}\right) - N_{\mathrm{y}} \ln\left(\frac{a_{\mathrm{y}}}{a_{\mathrm{y},1}}\right) - n \ln a_{\mathrm{w}} \tag{7}$$

Where $n = n_{\mathrm{s}} + n_{\mathrm{ls}}$ is the total number of molecules in the germ, and $a_{\mathrm{w},1}$ and $a_{\mathrm{y},1}$ are the activites of water and solute in the inital stage (Fig. 1), respectively. If the droplet size is much larger than the ice germ, which is almost always the case for ice nucleation, then $a_{\mathrm{w}} \approx a_{\mathrm{w},1}$ and $a_{\mathrm{y}} \approx a_{\mathrm{y},1}$, and to a good approximation,

$$\Delta G_{\mathrm{sln}} \approx -n k_{\mathrm{B}} T \ln a_{\mathrm{w}} \tag{8}$$

2.1 Energy of formation of the interface

To further develop Eq. (4) it is necessary to introduce a model of the solid–liquid interface. Theoretical models show that the solid–liquid interface is characterized by the organization of randomly moving liquid molecules into positions determined by the solid matrix (Spaepen, 1975; Karim and Haymet, 1988; Haymet and Oxtoby, 1981). Associated with this increased order is a decrease in the partial molar entropy of the liquid

ACPD
14, 1525–1557, 2014

molecules. Since the solid determines the positions of the molecules at the interface, the partial molar entropy at the interface must approximate the entropy of the solid. However the interface molecules are liquid-like, and their enthalpy remains that of the bulk liquid (Black, 2007). This implies that the system must pay the maximum entropic cost during the formation of the germ (Spaepen, 1975; Black, 2007). The entropic nature of the thermodynamic barrier for nucleation has been confirmed by molecular dynamics simulations (Reinhardt and Doye, 2013). This conceptual model is used below to develop an expression for the energy of formation of the interface.

The change in the partial molar free energy of water associated with the formation of the interface is given by

$$\mu_{\mathrm{w,ls}} - \mu_{\mathrm{w,2}} = h_{\mathrm{w,ls}} - T s_{\mathrm{w,ls}} - \mu_{\mathrm{w,2}} \tag{9}$$

Where $s_{\mathrm{w,ls}}$ is the entropy of the interface molecules. Assuming that the entropy of the molecules at the interface approximates the entropy of the bulk solid, i.e., $s_{\mathrm{w,ls}} \approx s_{\mathrm{w,s}}$, Eq. (9) can be written as,

$$\mu_{\mathrm{w,ls}} - \mu_{\mathrm{w,2}} = h_{\mathrm{w,ls}} - T s_{\mathrm{w,s}} - \mu_{\mathrm{w,2}} \tag{10}$$

Taking into account that $\mu_{\mathrm{w,s}} = h_{\mathrm{w,s}} - T s_{\mathrm{w,s}}$, and using Eq. (6) into Eq. (10) we obtain

$$\mu_{\mathrm{w,ls}} - \mu_{\mathrm{w,2}} = -k_{\mathrm{B}} T \ln\left(\frac{a_{\mathrm{w}}}{a_{\mathrm{w,eq}}}\right) + \Delta h_{\mathrm{w,ls}} \tag{11}$$

where $\Delta h_{\mathrm{w,ls}} = h_{\mathrm{w,ls}} - h_{\mathrm{w,s}}$ is the excess enthalpy of the molecules at the interface.

If no solute is present the enthalpy of the molecules at the interface approximates the enthalpy of water in the bulk, i.e, $\Delta h_{\mathrm{w,ls}} \approx \Delta h_{\mathrm{f}}$ where Δh_{f} is the latent heat of fusion of water. However the adsorption of solute at the interface affects $\Delta h_{\mathrm{w,ls}}$. Using the Gibbs model of adsorption the effect of the solute on $\Delta h_{\mathrm{w,ls}}$ can be accounted for in the form (Hiemenz and Rajagopalan, 1997; Gibbs, 1957),

$$\Delta h_{\mathrm{w,ls}} = \Delta h_{\mathrm{f}} - \Gamma_{\mathrm{w}} k_{\mathrm{B}} T \ln a_{\mathrm{w}} - \Gamma_{\mathrm{y}} k_{\mathrm{B}} T \ln a_{\mathrm{y}} \tag{12}$$

ACPD
14, 1525–1557, 2014

where Γ_w and Γ_y are the surface excess of water and solute, respectively, and represent the ratio of the number of molecules in the interface to the number of molecules at the dividing surface. According to the Gibbs model, Γ_w and Γ_y depend on the position of the dividing surface, which is arbitrary but typically chosen so that the surface excess of solvent is zero (Kashchiev, 2000). However by choosing the dividing surface as equimolecular with respect to the solute (Sect. 2) the resulting expressions become independent of the nature of the solute. Thus making $\Gamma_y = 0$, Eq. (12) becomes,

$$\Delta h_{w,ls} = \Delta h_f - \Gamma_w k_B T \ln a_w \tag{13}$$

In the solid matrix the number of molecules at the surface is given by $sn^{2/3}$ where s is a geometric constant depending on the crystal lattice (1.12 for hcp crystals and 1.09 for bcc crystals Jian et al., 2002), and n is the total number of atoms in the germ. However the ice germ is allowed to have any shape, as long as it has a defined lattice structure. The interface is generally made of several layers beyond the outer layer of the solid (Henson and Robinson, 2004; Chen and Crutzen, 1994; Spaepen, 1975). Spaepen (1975) showed that for random coverage of a solid matrix there are about 1.46 molecules at the interface for each molecule in the outer layer of the solid matrix. With this, $\Gamma_w = 1.46s$ and $n_{ls} = 1.46sn^{2/3}$. Equation (13) then becomes,

$$\Delta h_{w,ls} = \Delta h_f - 1.46 s k_B T \ln a_w \tag{14}$$

Introducing Eq. (14) into Eq. (11) we obtain,

$$\mu_{w,ls} - \mu_{w,2} = -k_B T \ln\left(\frac{a_w}{a_{w,eq}}\right) + \Delta h_f - 1.46 s k_B T \ln a_w \tag{15}$$

Equation (15) expresses the energy cost associated with the formation of the interface accounting for solute effects. Since it results from the consideration of the entropy reduction (i.e., negentropy production; Spaepen, 1994) across the interface, this model will be referred to as the Negentropic Nucleation Framework (NNF).

ACPD
14, 1525–1557, 2014

2.2 Nucleation work and nucleation rate

Introducing Eqs. (6), (8) and (15) into Eq. (4), and rearranging we obtain

$$\Delta G = -nk_{\mathrm{B}}T \ln\left(\frac{a_{\mathrm{w}}^2}{a_{\mathrm{w,eq}}}\right) + 1.46sn^{2/3}(\Delta h_{\mathrm{f}} - 1.46sk_{\mathrm{B}}T \ln a_{\mathrm{w}}) \tag{16}$$

where $n = n_{\mathrm{s}} + n_{\mathrm{ls}}$ was used.

The germ size at nucleation, n^*, and the nucleation work, ΔG_{nuc}, are obtained by applying the condition of mechanical equilibrium to Eq. (16), i.e.,

$$\frac{\mathrm{d}\Delta G_{\mathrm{nuc}}}{\mathrm{d}n^*} = -k_{\mathrm{B}}T \ln\left(\frac{a_{\mathrm{w}}^2}{a_{\mathrm{w,eq}}}\right) + \frac{2}{3}1.46s(n^*)^{-1/3}(\Delta h_{\mathrm{f}} - 1.46sk_{\mathrm{B}}T \ln a_{\mathrm{w}}) = 0 \tag{17}$$

Solving Eq. (17) for n^* and rearranging gives,

$$n^* = \frac{8}{27}\left[\frac{1.46s(\Delta h_{\mathrm{f}} - 1.46sk_{\mathrm{B}}T \ln a_{\mathrm{w}})}{k_{\mathrm{B}}T \ln\left(\frac{a_{\mathrm{w}}^2}{a_{\mathrm{w,eq}}}\right)}\right]^3 \tag{18}$$

The nucleation work is obtained by replacing Eq. (18) into Eq. (16). After rearranging we obtain,

$$\Delta G_{\mathrm{nuc}} = \frac{4}{27}\frac{[1.46s(\Delta h_{\mathrm{f}} - 1.46sk_{\mathrm{B}}T \ln a_{\mathrm{w}})]^3}{\left[k_{\mathrm{B}}T \ln\left(\frac{a_{\mathrm{w}}^2}{a_{\mathrm{w,eq}}}\right)\right]^2} \tag{19}$$

The nucleation rate, J_{hom}, is given by,

$$J_{\mathrm{hom}} = J_0 \exp\left(-\frac{\Delta G_{\mathrm{nuc}}}{k_{\mathrm{B}}T}\right) \tag{20}$$

ACPD
14, 1525–1557, 2014

where J_0 is a T-dependent preexponential factor. As in CNT, it is assumed that J_0 results from the kinetics of aggregation of single water molecules to the ice germ from an equilibrium cluster population (Kashchiev, 2000), therefore,

$$J_0 = \frac{N_c k_B T}{h} \frac{\rho_w}{\rho_i} \frac{Z \Omega_g}{v_w} \exp\left(-\frac{\Delta G_{act}}{k_B T}\right) \tag{21}$$

where N_c is the number of atoms in contact with the ice germ, ρ_w and ρ_i are the bulk liquid water and ice density, respectively, Ω_g is the germ surface area, and ΔG_{act} is the activation energy of the water molecules in the bulk of the liquid. Z is the Zeldovich factor, given by

$$Z = \left[\frac{\Delta G_{nuc}}{3\pi k_B T (n^*)^2}\right]^{1/2} \tag{22}$$

2.3 Classical Nucleation Theory

CNT is commonly used to described homogeneous ice nucleation (Khvorostyanov and Curry, 2004) and is therefore important to compare the NNF model against CNT predictions. According to CNT, the work of nucleation, ΔG_{CNT}, is given by (Pruppacher and Klett, 1997),

$$\Delta G_{CNT} = \frac{16\pi \sigma_{iw}^3 v_w^2}{3(k_B T \ln S_i)^2} \tag{23}$$

where $S_i = a_w \left(p_{s,w}/p_{s,i}\right)$, is the saturation ratio with respect to the ice phase. The critical germ size is given by,

$$n^*_{CNT} = \frac{32\pi \sigma_{iw}^3 v_w^2}{3(k_B T \ln S_i)^3} \tag{24}$$

ACPD
14, 1525–1557, 2014

The nucleation rate for CNT is obtained by replacing Eq. (24) into Eq. (19).

$$J_{\mathrm{CNT}} = J_0 \exp\left(-\frac{\Delta G_{\mathrm{CNT}}}{k_{\mathrm{B}}T}\right) \tag{25}$$

where J_0 is defined as in Eq. (21).

The usage Eq. (25) requires a parameterization of σ_{iw}, for which there is large uncertainty. Theoretical approaches have been developed to estimate σ_{iw} however they are mostly applicable to low undercooling (e.g., Digilov, 2004; Spaepen, 1994) and σ_{iw} is in general found by fitting J_{CNT} to experimental measurements of J_{hom} (e.g., Murray et al., 2010a; Khvorostyanov and Curry, 2004; Marcolli et al., 2007). Two approaches are employed to parameterize σ_{iw}. Following Murray et al. (2010a), the following correlation was used to describe σ_{iw},

$$\sigma_{\mathrm{iw}}(T) = 0.0229\left(\frac{T}{236.0}\right)^{0.97} (\mathrm{J\,m^{-2}}) \tag{26}$$

With T in K. The parameters of the correlation in Eq. (26) were slightly modified from the ones used by Murray et al. (2010a) to match the freezing point of pure water measured by Koop et al. (2000). The model presented in Sect. 2 however indicates that besides T, σ_{iw} must also depend on a_{w} since the presence of the solute in the interface layer modifies the interfacial energy. To account for this, a correlation for σ_{iw} was obtained by fitting J_{CNT} (Eq. 25) to the data of Koop et al. (2000) in the form,

$$\sigma_{\mathrm{iw}}(T, a_{\mathrm{w}}) = 0.00211 - 0.0513a_{\mathrm{w}} + 3.04 \times 10^{-4}T\,(\mathrm{J\,m^{-2}}) \tag{27}$$

With $180 < T < 273$ in K. The linear dependency of σ_{iw} on T is consistent with theoretical studies (Spaepen, 1994; Pruppacher and Klett, 1997). In agreement with experimental measurements (Pruppacher and Klett, 1997; Digilov, 2004), Eq. (27) predicts $\sigma_{\mathrm{iw}} = 33.9\,\mathrm{J\,m^{-2}}$ for $T = 273\,\mathrm{K}$ and $a_{\mathrm{w}} = 1$. Alpert et al. (2011) also fitted CNT results to K00, although no parameterization was reported. Comparison of selected values of σ_{iw} from Alpert et al. (2011) against Eq. (27) shows reasonable agreement (not shown).

ACPD
14, 1525–1557, 2014

3 Discussion

3.1 Nucleation rate

Figure 2 shows the nucleation rate calculated from K00 and the NNF and CNT models, i.e., Eqs. (20) and (25). For NNF, the surface area parameter, s, in Eq. (19) was set to 1.105, that is, the ice germ structure is assumed to lie somewhere between a bcc ($s = 1.12$) and a hcp ($s = 1.109$) crystal, justified on experimental studies showing that ice forms as a stacked disordered structure (Malkin et al., 2012). The values used for the parameters of Eqs. (19) and (20) are listed in Table A1. CNT results are shown using Eqs. (26) and (27) to calculate σ_{iw}. The correlation of Koop and Zobrist (2009) was used to calculate $a_{w,eq}$. The experimental results of Murray et al. (2010a) (M10) and Riechers et al. (2013)(R13) are also included in Fig. 2. Murray et al. (2010a) compared experimentally determined nucleation rates from several sources and found about a factor of 10 variation in J_{hom} of pure water. Riechers et al. (2013) recently developed a new experimental technique based on microfluidics to measure J_{hom}. Although these correlations are only applicable around 236 K, they are included as reference for the limiting case of $a_w = 1$.

The freezing temperature, T_f, was calculated by solving,

$$J_{hom}(T_f)\Delta t v_d = 1 \tag{28}$$

where Δt is the experimental time scale and v_d the droplet volume. Equation (28) represents a freezing fraction of about 63 % for a monodisperse droplet distribution or 50 % for a lognormal distribution (Barahona, 2012). T_f is calculated by numerical iteration and assuming $\Delta t = 10$ s and a mean droplet diameter of 10 µm, selected to match to the conditions used by Koop et al. (2000).

Except for R13 there is overlap between all the curves of Fig. 2 for T around 236 K, that is, near the homogeneous freezing T of pure water ($a_w = 1$). This is in agreement with the study of Murray et al. (2010a) showing that most models predict similar J_{hom} for pure water. R13 predicts about three orders of magnitude lower J_{hom} than the other

ACPD
14, 1525–1557, 2014

models of Fig. 2. A similar behavior was found in Riechers et al. (2013) which was ascribed to experimental inaccuracy in previous studies, although no independent works have corroborated their conclusions.

For $T < 236$ K and $a_w < 1$, Fig. 2 shows significant differences in predicted nucleation rates. For $J_{hom} \lesssim 10^{15}$ the NNF and K00 models agree within within the typical scatter of experimentally determined J_{hom} (e.g., Murray et al., 2010b; Alpert et al., 2011). However they diverge for $J_{hom} \gtrsim 10^{15}$ for which K00 tends to grow much quickier than for CNT and NNF (Figs. 2 and 4). When Eq. (27) is used to parameterize σ_{iw}, J_{hom} from CNT shows good agreement with K00; this is however by design as K00 was used to generate Eq. (27). When Eq. (26) is used to parameterize σ_{iw}, J_{hom} from CNT is much lower than predicted by either NNF and K00, and only at $a_w = 1$ J_{hom} from CNT agrees with experimental observations. Such high sensitivity to σ_{iw} is one of the main drawbacks of CNT.

NNF and CNT show an initial increase in J_{hom} as T decreases however this tendency eventually reverses at low T. This behavior is caused by an increase in ΔG_{act} as T decreases, i.e., the role of activation of water molecules becomes increasingly more significant at low T limiting J_{hom} (Sect. 3.3). In contrast, the K00 parameterization shows a monotonical increase in J_{hom} as T decreases. An explanation for this behavior may be found in the experimental method used to generate the K00 parameterization. Optical methods are accurate at low J_{hom} where the freezing of individual droplets can be easily discriminated. However they are inherently limited to temperatures below which the droplet freezing fraction, f_f, becomes unity. Nucleation rates that would produce $f_f > 1$ are not measured directly but extrapolated from measurements at lower f_f. Thus the maximum and subsequent reduction in J_{hom} as T decreases at constant a_w (Fig. 2) may be difficult to infer from observation of the freezing of single droplets. It is plausible that the K00 parameterization overestimates the highest values of J_{hom}. Numerical test (not shown) suggest that this may lead to overestimation of droplet freezing fractions particularly for small droplets, although it has a limited impact in ambient clouds where f_f is typically small (Barahona and Nenes, 2008).

ACPD
14, 1525–1557, 2014

3.2 Critical germ size

Figure 3 shows the critical germ size in terms of number of water molecules, calculated using NNF and CNT. According to the nucleation theorem (Kashchiev, 2000), n^* can also be determined directly from experimental results following,

$$n^* = -\frac{\mathrm{d}\Delta G_{\mathrm{nuc}}}{\mathrm{d}\Delta\mu_{\mathrm{w}}} + \frac{\partial\Phi}{\partial\Delta\mu_{\mathrm{w}}} \tag{29}$$

where Φ is the energy of formation of the interface, and $\Delta\mu_{\mathrm{w}} = -k_{\mathrm{B}}T\ln\left(\frac{a_{\mathrm{w}}}{a_{\mathrm{w,eq}}}\right)$. Equation (29) can be simplified in the form (Kashchiev, 2000),

$$n^* = \frac{\mathrm{d}\ln J_{\mathrm{hom}}}{\mathrm{d}\ln a_{\mathrm{w}}} - 1 \tag{30}$$

where it is assumed that Φ, or equivalently σ_{iw}, does not depend on a_{w}. Using the K00 parameterization into Eq. (30) results in n^* between 400 and 600 molecules for T between 190 K and 236 K (Fig. 3). On the other hand, NNF (Eq. 18) predicts n^* around 260 for the same T interval and CNT around 100 (Eq. 24). A similar discrepancy between K00 and CNT was found by Ford (2001) who ascribed it to deficiencies in CNT. However NNF offers further insight into the origin of the differences in n^*.

Figure 4 suggests that around the freezing a_{w} (defined in a similar way as T_{f} in Eq. 28), $\frac{\mathrm{d}\ln J_{\mathrm{hom}}}{\mathrm{d}\ln a_{\mathrm{w}}}$ is similar in K00 and CNT (with σ_{iw} as defined in Eq. 27) although lower than in NNF. The fact that n^* is higher for K00 than for NNF (Fig. 3), even though $\frac{\mathrm{d}\ln J_{\mathrm{hom}}}{\mathrm{d}\ln a_{\mathrm{w}}}$ is higher in the latter, is at odds with the predictions of Eq. (30). This picture can only be reconciled if $\frac{\partial\Phi}{\partial\Delta\mu_{\mathrm{w}}} \neq 0$, that is, the interfacial energy must depend on a_{w}, which is also suggested by Eq. (19). This dependency is explicit in the NNF model (Sect. 2.1). In CNT, it can be introduced by making σ_{iw} a function of a_{w} (Eq. 27).

To explain the dependency of the interfacial energy on a_{w} one must consider the Gibbs model of the interface (Sect. 2.1). By introducing the arbitrary dividing surface,

ACPD
14, 1525–1557, 2014

an excess number of molecules is created around the interface between the liquid and the solid (Hiemenz and Rajagopalan, 1997). This is typically dealt with by selecting the so-called equimolecular dividing surface (EDS), in which the interface has energy but its net molecular excess is zero (Kashchiev, 2000; Schay, 1976). However the EDS cannot be defined simultaneously for the solute and the solvent. In fact, using the EDS with respect to the solvent, results in a molecular excess of solute at the interface which is not taken into account in CNT. This explains the discrepancy in n^* between Eq. (30) and CNT. In Sect. 2 it is shown that it is advantageous to define the EDS with respect to the solute, and account explicitly for the excess of water molecules at the interface. Thus the consistency between the choice of the dividing surface and the molecular excess at the interface is explicit in NNF. This picture also implies that Eq. (29) (which does not depend on the choice of the dividing surface) instead of Eq. (30), must be used in the analysis of ice nucleation data.

It is also important to test whether the picture presented in Sect. 2.1 is physically reasonable. The pressure change across the interface can be calculated using the generalized Laplace equation (Kashchiev, 2000),

$$\Delta P = \frac{1}{v_\mathrm{w}} \frac{\partial \Phi}{\partial n^*} \tag{31}$$

where the solid is assumed incompressible. Direct application of Eq. (31) is somehow difficult because a_w is not independent of n^*. However at $a_\mathrm{w} = 1$ this can be simplified since n^* is only dependent on T. Thus, making $\Phi = (\mu_{\mathrm{w,ls}} - \mu_{\mathrm{w},2}) n_\mathrm{ls}$ and replacing Eq. (15) into Eq. (31) we obtain for $a_\mathrm{w} = 1$,

$$\Delta P(a_\mathrm{w} = 1) = \frac{2}{3} \frac{1.46 s \Delta h_\mathrm{f}}{v_\mathrm{w} (n^*)^{1/3}} \tag{32}$$

Using the parameters of Table A1, $\Delta P = 336$ bar for $n^* = 260$. This value is below the compressibility limit of water (Baker and Baker, 2004). Thus the picture of the interface proposed here, although an approximation, is physically plausible. ΔP is of the same

ACPD
14, 1525–1557, 2014

order as the osmotic pressure defined by Baker and Baker (2004), however the relation between ΔP and the osmotic pressure is not clear.

3.3 Freezing temperature

Finally we investigate whether the model presented in Sect. 2 is able to explain the water activity criteria of Koop et al. (2000). Figure 5 shows the freezing T defined by Eq. (28), calculated using K00, CNT and NNF. Results using the correlation of Bullock and Molinero (2013) (hereafter BM13) derived from MD simulations are also included. The gray area in Fig. 5 is obtained by setting $\Delta a_w = 0.313 \pm 0.025$ and represents the typical range of experimental observations (Koop and Zobrist, 2009; Alpert et al., 2011; Knopf and Rigg, 2011). T_f for K00 was obtained by solution of Eq. (28), resulting in an average Δa_w of 0.302. The slightly lower Δa_w than reported by Koop and Zobrist (2009) ($\Delta a_w = 0.313$) results from using a fixed droplet size of 10 µm whereas in Koop et al. (2000) D_p varied between 1 µm and 10 µm.

For CNT, using σ_{iw} corrected for a_w effects results in agreement with K00, which however is by design as T_f predicted by K00 was used to specify σ_{iw} (Eq. 27). Using σ_{iw} from Eq. (26) which is based on a fit to observed T_f at $a_w = 1$ results in overprediction of T_f for $a_w < 1$. For $T_f > 200$ K, BM13 agrees with K00 within the experimental uncertainty, but it tends to overpredict T_f for lower temperature. This overprediction was also observed by Bullock and Molinero (2013) and was ascribed to the temperature dependency of the water activity coefficient. T_f from K00 and NNF overlap down to 190 K (Fig. 5). For $T < 190$ K, NNF tends to predict lower T_f than K00 although within the range of experimental observations. Since no data from K00 are used in NNF, the model developed here constitutes an independent theoretical explanation of the results of Koop et al. (2000).

ACPD
14, 1525–1557, 2014

Using NNF Δa_w, can be obtained by solving,

$$k_B T \ln(J_0 \Delta t v_d) - \frac{4}{27} \frac{\left\{1.46 s \left[\Delta h_f - 1.46 s k_B T \ln(a_{w,eq} + \Delta a_w)\right]\right\}^3}{\left\{k_B T \ln\left[\frac{(a_{w,eq}+\Delta a_w)^2}{a_{w,eq}}\right]\right\}^2} = 0 \tag{33}$$

Equation (33) was obtained by replacing Eq. (20) into Eq. (28). Since the roots of Eq. (33) determine T_f, it is termed the characteristic freezing function.

Inspection of Eq. (33) shows that it is a function of T only, since the a_w dependency is removed by application of Eq. (28). Thus, the roots of Eq. (33) are determined by the value of Δa_w. Figure 6 shows that Eq. (33) only has real solutions in the interval $185\,\mathrm{K} < T < 238\,\mathrm{K}$ over a very narrow set of values of Δa_w, i.e., $0.298 < \Delta a_w < 0.306$. Thus for T_f to exist, Δa_w must be almost constant. This is the origin of the water activity criteria since the variation in Δa_w shown in Fig. 6 is well within experimental uncertainty (Fig. 5). An interesting feature of Eq. (33) is that it produces similar $T - a_w$ curves for different Δa_w values. This means that the multiple roots of Eq. (33) are located at similar T_f for different values of Δa_w, and always fall on the same curve.

Figure 6 shows that Eq. (33) constitutes a theoretical derivation of the water activity criteria. Δa_w can be obtained by numerically solving Eq. (33). However for $a_w = 1$, Eq. (33) is simplified and Δa_w can be found by direct analytical solution, in the form,

$$\Delta a_w = 1 - \exp\left[-\frac{2}{3\sqrt{3\ln(J_0 \Delta t v_d)}} \left(\frac{\Delta h_f}{k_B T^*}\right)^{3/2}\right] = 0.304 \tag{34}$$

where $T^* = 236.03$ is the freezing temperature at $a_w = 1$. The value of Δa_w in Eq. (34) was obtained using the parameters of Table A1 calculated at T^*. Δa_w is very close to the value of 0.302 found by application of K00 (Fig. 5) and within experimental uncertainty of reported values (e.g., Koop and Zobrist, 2009; Alpert et al., 2011). For $T > 190\,\mathrm{K}$, Δa_w calculated from Eq. (33) is fairly constant (being 0.300 at $T = 190\,\mathrm{K}$). For $T < 190$ there is a slight increase in Δa_w reaching about 0.31 at $T = 180\,\mathrm{K}$. This increase is due

ACPD
14, 1525–1557, 2014

to the increase in ΔG_{act} at low T. J_{hom} at very low T is still uncertain, since factors like the formation of glasses (Murray et al., 2010b) and the formation of highly concentrated brines within droplets may play a role (Bogdan and Molina, 2010; Swanson, 2009).

From the agreement of BM13 with K00 (Fig. 5) Bullock and Molinero (2013) concluded that the formation of four-coordinated water controls T_f, which implies a kinetic control for nucleation. This view can be reconciled with the thermodynamic framework presented here by taking into account the role of ΔG_{act} in determining J_{hom}. The product $\frac{N_c k_B T}{h}\frac{\rho_w}{\rho_i}\frac{Z\Omega_g}{v_w}$ in Eq. (21) is almost constant between 180 K and 236 K. Therefore the flux of molecules to the germ is controlled by ΔG_{act}. In fact, by replacing Eq. (19) into Eq. (20) and then into Eq. (28), we obtain after rearranging,

$$\frac{\Delta G_{nuc} + \Delta G_{act}}{T_f} \approx \text{constant} \tag{35}$$

Thus an increase ΔG_{act} is balanced by a decrease in ΔG_{nuc}, i.e., the increase in the driving force for nucleation at low T makes up for the decrease in the mobility of water molecules. One can hypothesize that the formation of low density patches of water within a supercooled droplet becomes less frequent at low a_w (hence low T_f), which translates into a larger ΔG_{act}. Hence ΔG_{act} exerts a kinetic control on T_f and ΔG_{nuc} responds accordingly (Eq. 35). In other words, a kinetic constraint to nucleation implies a thermodynamic one (and vice versa), and T_f represents the temperature at which they balance. ΔG_{act} is closely related to the self-diffusivity of water (Pruppacher and Klett, 1997) thus it follows that diffusivity must play critical role in determining J_{hom}. This is quite different from the classical picture that considers the preexponential factor in Eq. (20) a constant, independent of T. Since ΔG_{nuc} can be defined over a purely thermodynamic basis (Sect. 2), Eq. (35) suggests that ΔG_{act} may also admit a thermodynamic description.

ACPD
14, 1525–1557, 2014

4 Conclusions

The model presented in Sect. 2 constitutes a new nucleation framework that does not use the interfacial tension as defining parameter. It is therefore free from biases induced by uncertainties in the parameterization of σ_{iw}. Instead, an expression for the interfacial energy was developed directly using thermodynamic principles. The new theory is based on a conceptual model in which the interface is considered to be made of "water molecules trapped by the solid matrix". It also accounts for the finite droplet size leading to changes in the composition of the liquid phase upon nucleation. Since it places emphasis on the increase in order and the reduction in entropy across the interface, the new model has been termed the Negentropic Nucleation Framework, NNF.

Comparison against experimental results showed that the new framework is able to reproduce measured nucleation rates and is capable of explaining the observed constant shift in water activity between melting and nucleation (Koop et al., 2000). The constant water activity shift originates because the freezing temperature only exist for a very narrow range of Δa_w (Eq. 33), and represents a balance between kinetic and thermodynamic constraints to nucleation. NNF shows that the effect of water activity on nucleation is a manifestation of the entropic barrier to the formation of the germ. An analytical expression for Δa_w was derived and was shown to agree well with the experimental value measured by Koop and Zobrist (2009). This constitutes the first phenomenological derivation of the water activity criteria found by Koop et al. (2000).

The new framework suggests that to reconcile experimental results and theoretical models the interfacial energy must depend on a_w. This is implicit in the development of NNF, however is missing in CNT. The dependency of J_{hom} on a_w originates from the excess concentration of either solute or solvent when the dividing surface is defined. Such excess is present even if the EDS is defined with respect to the solvent. It was shown that it is advantageous to define the EDS with respect to the solute because the resulting expressions are independent of the nature of the solute, and therefore

ACPD
14, 1525–1557, 2014

consistent with experimental observations. Although such considerations are neglected in CNT, it was shown that CNT can be corrected by allowing σ_{iw} to depend on a_w, for which a new empirical correlation was developed.

Analysis of the new framework suggested that the temperature dependency of both the kinetic and thermodynamic terms plays a significant role in defining J_{hom} and T_f. It was shown that around T_f the increase in ΔG_{act} as T decreases is compensated by a decrease in ΔG_{nuc}. Thus an increased driving force for nucleation compensates the slower molecular diffusion at low T. Such coupling between kinetics and thermodynamics during nucleation suggests that a thermodynamic description of the preexponential factor (Eq. 20) may be possible.

Some disparity was found between the K00 parameterization and NNF for $T < 185$ K. This may be ascribed to non-equilbrium effects and the possible formation of glasses at low T. Further research is required to elucidate the mechanism of freezing at such low T. The model presented here emphasizes the entropic nature of homogeneous nucleation. Molecular simulations may shed further light on the role of entropy changes across the interface on ice nucleation. Measurements of the interface thickness would also help elucidate the role of the ice crystal lattice structure (represented by the constant s in Eq. 15) in determining J_{hom}.

The framework presented here reconciles theoretical and experimental results. It will also help reduce the uncertainty in J_{hom} associated with the parameterization of σ_{iw} in theoretical models. It offers for the first time a thermodynamically consistent explanation of the effect of water activity on ice nucleation. Its relative simplicity makes it suitable to describe ice nucleation in the atmospheric models, and may lead to a better understanding of the formation of ice in the atmosphere.

Acknowledgements. Donifan Barahona was supported by the NASA Modeling, Analysis and Prediction program under WBS 802678.02.17.01.07. The author thanks Athanasios Nenes for his comments on the manuscript.

ACPD
14, 1525–1557, 2014

References

Alpert, P. A., Aller, J. Y., and Knopf, D. A.: Initiation of the ice phase by marine biogenic surfaces in supersaturated gas and supercooled aqueous phases, Phys. Chem. Chem. Phys., 13, 19882–19894, 2011. 1528, 1529, 1536, 1538, 1541, 1542, 1556

Baker, M. and Baker, M.: A new look at homogeneous freezing of water, Geophys. Res. Lett., 31, L19102, doi:10.1029/2004GL0204, 2004. 1529, 1540, 1541

Barahona, D.: On the ice nucleation spectrum, Atmos. Chem. Phys., 12, 3733–3752, doi:10.5194/acp-12-3733-2012, 2012. 1537

Barahona, D. and Nenes, A.: Parameterization of cirrus formation in large scale models: homogeneous nucleation, J. Geophys. Res., 113, D11211, doi:10.1029/2007JD009355, 2008. 1528, 1538

Barahona, D. and Nenes, A.: Dynamical states of low temperature cirrus, Atmos. Chem. Phys., 11, 3757–3771, doi:10.5194/acp-11-3757-2011, 2011. 1526

Barahona, D., Rodriguez, J., and Nenes, A.: Sensitivity of the global distribution of cirrus ice crystal concentration to heterogeneous freezing, J. Geophys. Res., 15, D23213, doi:10.1029/2010JD014273, 2010. 1528

Barahona, D., Molod, A., Bacmeister, J., Nenes, A., Gettelman, A., Morrison, H., Phillips, V., and Eichmann, A.: Development of two-moment cloud microphysics for liquid and ice within the NASA Goddard earth observing system model (GEOS-5), Geosci. Model Dev. Discuss., 6, 5289–5373, doi:10.5194/gmdd-6-5289-2013, 2013. 1526

Bauerecker, S., Ulbig, P., Buch, V., Vrbka, L., and Jungwirth, P.: Monitoring ice nucleation in pure and salty water via high-speed imaging and computer simulations, J. Phys. Chem. C, 112, 7631–7636, 2008. 1527, 1530

Black, S.: Simulating nucleation of molecular solids, P. R. Soc. A, 463, 2799–2811, 2007. 1531, 1532

Bogdan, A. and Molina, M.: Aqueous aerosol may build up an elevated upper tropospheric ice supersaturation and form mixed-phase particles after freezing, J. Phys. Chem. A, 114, 2821–2829, 2010. 1543

Bourne, J. and Davey, R.: The role of solvent-solute interactions in determining crystal growth mechanisms from solution: I. The surface entropy factor, J. Cryst. Growth, 36, 278–286, 1976. 1531

ACPD
14, 1525–1557, 2014

Brukhno, A. V., Anwar, J., Davidchack, R., and Handel, R.: Challenges in molecular simulation of homogeneous ice nucleation, J. Phys.-Condens. Mat., 20, 494243, doi:10.1088/0953-8984/20/49/494243, 2008. 1527

Bullock, G. and Molinero, V.: Low-density liquid water is the mother of ice: on the relation between mesostructure, thermodynamics and ice crystallization in solutions, Faraday Discuss., 167, 371–382, doi:10.1039/C3FD00085K, 2013. 1527, 1529, 1541, 1543, 1556

Chen, J.-P. and Crutzen, P. J.: Solute effects on the evaporation of ice particles, J. Geophys. Res., 99, 18847–18859, 1994. 1533

Digilov, R. M.: Semi-empirical model for prediction of crystal–melt interfacial tension, Surf. Sci., 555, 68–74, 2004. 1527, 1536

Dufour, L. and Defay, R.: Thermodynamics of Clouds, International Geophysics Series, vol. 6, . Academic Press, New York, 1963. 1527

Errington, J. R., Debenedetti, P. G., and Torquato, S.: Cooperative origin of low-density domains in liquid water, Phys. Rev. Lett. 89, 215503, doi:10.1103/PhysRevLett.89.215503, 2002. 1527

Ford, I. J.: Properties of ice clusters from an analysis of freezing nucleation, J. Phys. Chem. B, 105, 11649–11655, 2001. 1539

Fu, Q.: An accurate parameterization of the solar radiative properties of cirrus clouds for climate models, J. Climate, 9, 2058–2082, 1996. 1526

Gettelman, A., Liu, X., Barahona, D., Lohmann, U., and Chen, C.: Climate impacts of ice nucleation, J. Geophys. Res., 117, D20201, doi:10.1029/2012JD017950, 2012. 1526

Gibbs, J. W.: The Collected Works of J. Willard Gibbs, Yale University Press, New Haven, USA, 1957. 1530, 1532

Hartmann, D., Holton, J., and Fu, Q.: The heat balance of the tropical tropopause, cirrus, and stratospheric dehydration, Geophys. Res. Lett., 28, 1969–1972, 2001. 1526

Haymet, A. and Oxtoby, D. W.: A molecular theory for the solid–liquid interface, J. Chem. Phys., 74, 2559, doi:10.1063/1.441326, 1981. 1531

Henson, B. and Robinson, J.: Dependence of quasiliquid thickness on the liquid activity: a bulk thermodynamic theory of the interface, Phys. Rev. Lett., 92, 246107, doi:10.1103/PhysRevLett.92.246107, 2004. 1533

Hiemenz, P. C. and Rajagopalan, R.: Principles of Colloid and Surface Chemistry, revised and expanded, vol. 14, CRC Press, New York, 1997. 1532, 1540

Jensen, E. and Pfister, L.: Transport and freeze-drying in the tropical tropopause layer, J. Geophys. Res., 109, D02207, doi:10.1029/2003JD004022, 2004. 1526

Jensen, E. J., Toon, O. B., and Hamill, P.: Homogeneous freezing nucleation of stratospheric solution droplets, Geophys. Res. Lett., 18, 1857–1860, 1991. 1528

Jian, Z., Kuribayashi, K., and Jie, W.: Solid–liquid interface energy of metals at melting point and undercooled state, Mater. Trans., 43, 721–726, 2002. 1533

Johari, G., Fleissner, G., Hallbrucker, A., and Mayer, E.: Thermodynamic continuity between glassy and normal water, J. Phys. Chem., 98, 4719–4725, 1994. 1551

Kärcher, B. and Lohmann, U.: A parameterization of cirrus cloud formation: homogeneous freezing including effects or aerosol size, J. Geophys. Res., 107, 4698, doi:10.1029/2001JD001429, 2002. 1528

Karim, O. A. and Haymet, A.: The ice/water interface: a molecular dynamics simulation study, J. Chem. Phys., 89, 6889, doi:10.1063/1.455363, 1988. 1531

Kashchiev, D.: Nucleation: Basic Theory with Applications, Butterworth Heinemann, Oxford, 2000. 1527, 1528, 1531, 1533, 1535, 1539, 1540

Khvorostyanov, V. and Curry, J.: Critical humidities of homogeneous and heterogeneous ice nucleation: inferences from extended classical nucleation theory, J. Geophys. Res., 114, D04207, doi:10.1029/2008JD011197, 2009. 1527

Khvorostyanov, V. I. and Curry, J. A.: Thermodynamic theory of freezing and melting of water and aqueous solutions, J. Phys. Chem. A, 108, 11073–11085, 2004. 1527, 1528, 1529, 1535, 1536

Knopf, D. A. and Rigg, Y. J.: Homogeneous ice nucleation from aqueous inorganic/organic particles representative of biomass burning: water activity, freezing temperatures, nucleation rates, J. Phys. Chem. A, 115, 762–773, 2011. 1528, 1541

Koop, T. and Zobrist, B.: Parameterizations for ice nucleation in biological and atmospheric systems, Phys. Chem. Chem. Phys., 11, 10839–10850, 2009. 1537, 1541, 1542, 1544, 1551, 1556

Koop, T., Luo, B., Tslas, A., and Peter, T.: Water activity as the determinant for homogeneous ice nucleation in aqueous solutions, Nature, 406, 611–614, 2000. 1528, 1529, 1536, 1537, 1541, 1544, 1553, 1554

Laaksonen, A., Talanquer, V., and Oxtoby, D. W.: Nucleation: measurements, theory, and atmospheric applications, Annu. Rev. Phys. Chem., 46, 489–524, 1995. 1527

Liu, X., Penner, J., Ghan, S., and Wang, M.: Inclusion of ice microphysics in the NCAR Community Atmospheric Model version 3 (CAM3), J. Climate, 20, 4526–4547, 2007. 1528

Lohmann, U. and Feichter, J.: Global indirect aerosol effects: a review, Atmos. Chem. Phys., 5, 715–737, doi:10.5194/acp-5-715-2005, 2005. 1526
Lohmann, U. and Kärcher, B.: First interactive simulations of cirrus clouds formed by homogeneous freezing in the ECHAM general circulation model, J. Geophys. Res., 107, 4105, doi:10.1029/2001JD000767, 2002. 1528
MacKenzie, A.: Are the (solid–liquid) Kelvin equation and the theory of interfacial tension components commensurate?, J. Phys. Chem. B, 101, 1817–1823, 1997. 1528
Malkin, T. L., Murray, B. J., Brukhno, A. V., Anwar, J., and Salzmann, C. G.: Structure of ice crystallized from supercooled water, P. Natl. Acad. Sci. USA, 109, 1041–1045, 2012. 1537
Marcolli, C., Gedamke, S., Peter, T., and Zobrist, B.: Efficiency of immersion mode ice nucleation on surrogates of mineral dust, Atmos. Chem. Phys., 7, 5081–5091, doi:10.5194/acp-7-5081-2007, 2007. 1528, 1536
Matsumoto, M., Saito, S., and Ohmine, I.: Molecular dynamics simulation of the ice nucleation and growth process leading to water freezing, Nature, 416, 409–413, 2002. 1527
Moore, E. B. and Molinero, V.: Structural transformation in supercooled water controls the crystallization rate of ice, Nature, 479, 506–508, 2011. 1527
Murphy, D. and Koop, T.: Review of the vapour pressures of ice and supercooled water for atmospheric applications, Q. J. Roy. Meteor. Soc., 131, 1539–1565, 2005. 1551
Murray, B., Broadley, S., Wilson, T., Bull, S., Wills, R., Christenson, H., and Murray, E.: Kinetics of the homogeneous freezing of water, Phys. Chem. Chem. Phys., 12, 10380–10387, 2010a. 1528, 1536, 1537, 1553
Murray, B., Wilson, T., Dobbie, S., Cui, Z., Al-Jumur, S., Mähler, O., Schnaiter, M., Wagner, R., Benz, S., Niemand, M., Saathoff, H., Ebert, V., Wagner, S., and Kärcher, B.: Heterogeneous nucleation of ice particles on glassy aerosol under cirrus conditions, Nat. Geosci., 3, 233–237, 2010b. 1527, 1538, 1543
Pruppacher, H. and Klett, J.: Microphysics of Clouds and Precipitation, 2nd edn., Kluwer Academic Publishers, Boston, MA, 1997. 1526, 1527, 1528, 1535, 1536, 1543, 1551
Reinhardt, A. and Doye, J. P.: Note: homogeneous TIP4P/2005 ice nucleation at low supercooling, J. Chem. Phys., 139, 096102, doi:10.1063/1.4819898, 2013. 1532
Riechers, B., Wittbracht, F., Hütten, A., and Koop, T.: The homogeneous ice nucleation rate of water droplets produced in a microfluidic device and the role of temperature uncertainty, Phys. Chem. Chem. Phys., 15, 5873–5887, 2013. 1528, 1537, 1538, 1553

ACPD
14, 1525–1557, 2014

Schay, G.: A comprehensive presentation of the thermodynamics of adsorption excess quantities, Pure Appl. Chem., 48, 393–400, 1976. 1540

Spaepen, F.: A structural model for the solid–liquid interface in monatomic systems, Acta Metall. Mater., 23, 729–743, 1975. 1531, 1532, 1533

Spaepen, F.: Homogeneous nucleation and the temperature dependence of the crystal-melt interfacial tension, Solid State Phys., 47, 1–32, 1994. 1533, 1536

Swanson, B. D.: How well does water activity determine homogeneous ice nucleation temperature in aqueous sulfuric acid and ammonium sulfate droplets?, J. Atmos. Sci., 66, 741–754, 2009. 1543

Tabazadeh, A., Jensen, E., and Toon, O.: A model description for cirrus cloud nucleation from homogeneous freezing of sulfate aerosols, J. Geophys. Res., 102, 23485–23850, 1997. 1528

Wang, B. and Knopf, D. A.: Heterogeneous ice nucleation on particles composed of humic-like substances impacted by O_3, J. Geophys. Res., 116, D03205, doi:10.1029/2010JD014964, 2011. 1528

Wu, D. T., Gránásy, L., and Spaepen, F.: Nucleation and the solid–liquid interfacial free energy, MRS Bull., 29, 945–950, 2004. 1527, 1528

Zobrist, B., Koop, T., Luo, B., Marcolli, C., and Peter, T.: Heterogeneous ice nucleation rate coefficient of water droplets coated by a nonadecanol monolayer, J. Phys. Chem. C, 111, 2149–2155, 2007. 1551

ACPD
14, 1525–1557, 2014

Table A1. List of symbols.

a_w, a_y	Activity of water and solute, respectively
$a_{w,eq}$	Equilibrium a_w between bulk liquid and ice (Koop and Zobrist, 2009)
f_f	Droplet freezing fraction
G	Gibbs free energy
h	Planck's constant
$h_{w,s}$, $h_{w,ls}$	Partial molar enthalpy of water in ice and at the interface, respectively
J_0	Preexponential factor
J_{hom}	Nucleation rate
k_B	Boltzmann constant
n	Total number of molecules in the solid germ
n^*	Critical germ size
n_s, n_{ls}	Number of molecules in the bulk of the solid and in the interface, respectively
N_c	Number of atoms in contact with the ice germ, $5.85 \times 10^{18}\ m^{-2}$ (Pruppacher and Klett, 1997)
N_w, N_y	Total number of water and solute molecules, respectively
$p_{s,w}$, $p_{s,i}$	Liquid water and ice saturation (Murphy and Koop, 2005)
s	Geometric constant relating n and n_{ls}
S_i	Saturation ratio with respect to ice
$s_{w,s}$, $s_{w,ls}$	Partial molar entropy of water in bulk ice and at the interface, respectively
T	Temperature
T_f	Freezing T
v_d	Droplet volume
v_w	Molecular volume of water in ice (Zobrist et al., 2007)
Z	Zeldovich factor
ΔG_{act}	Activation energy of liquid water (Zobrist et al., 2007)
ΔG_{nuc}	Nucleation work
ΔG_{sln}	Change in free energy of the bulk solution during nucleation
$\Delta h_{w,ls}$	Excess enthalpy of the interface
Δh_f	Heat of fusion of water*
Δt	Experimental time scale
Δa_w	$a_w - a_{w,eq}$
Φ	Energy of formation of the interface
Γ_w, Γ_y	Molecular surface excess of water and solute, respectively
μ_w, μ_y	Chemical potential of water and solute, respectively
$\mu_{w,ls}$	Chemical potential of water at the interface
$\mu_{w,s}$	Chemical potential of bulk ice
ρ_w, ρ_i	Bulk density of liquid water and ice, respectively (Pruppacher and Klett, 1997)
σ_{iw}	Ice-liquid interfacial energy
Ω_g	Ice germ surface area

* From the data of Johari et al. (1994) the following fit was obtained:
$\Delta h_f = 7.50856 \times 10^{-7} T^5 - 8.40025 \times 10^{-4} T^4 + 0.367171 T^3 - 78.1467 T^2 + 8117.02 T - 3.29032 \times 10^5\ (\mathrm{J\,mol^{-1}})$ for T between 180 K and 273 K.

ACPD
14, 1525–1557, 2014

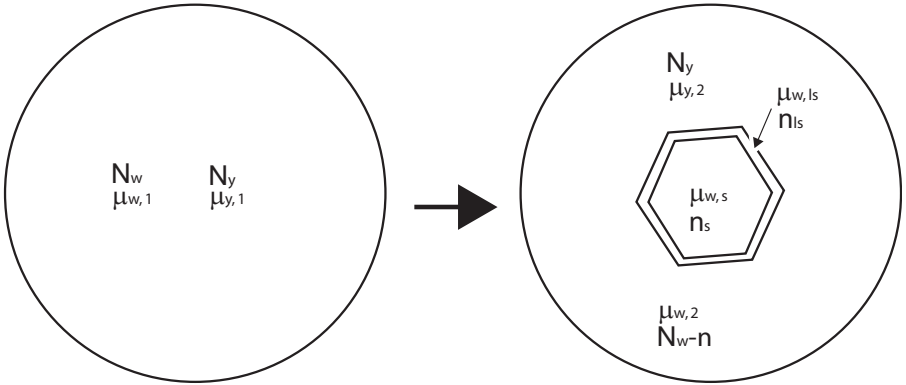

Fig. 1. Scheme of the formation of an ice germ from a liquid phase. Subscripts 1 and 2 represent the state of the system before and after germ formation, respectively. N_w and N_y represent the total molecular concentration of water and solute in the system, respectively. The subscripts ls and s refer to the liquid–solid interface and solid phases, respectively.

ACPD
14, 1525–1557, 2014

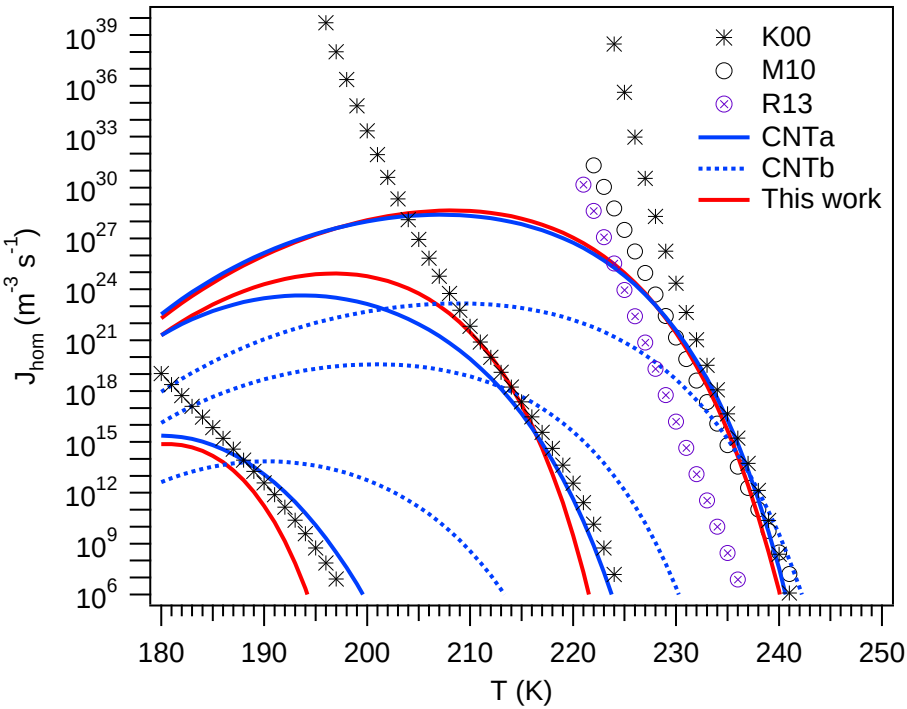

Fig. 2. Homogeneous nucleation rate. K00, M10 and R13 refer to results obtained using the correlations of Koop et al. (2000), Murray et al. (2010a) and Riechers et al. (2013), respectively. For CNT σ_{iw} was calculated using either Eq. (27) (line CNTa) or Eq. (26) (line CNTb). Lines are grouped by increasing water activity: a_w = 0.8, 0.9 and 1.0, from left to right, respectively.

ACPD
14, 1525–1557, 2014

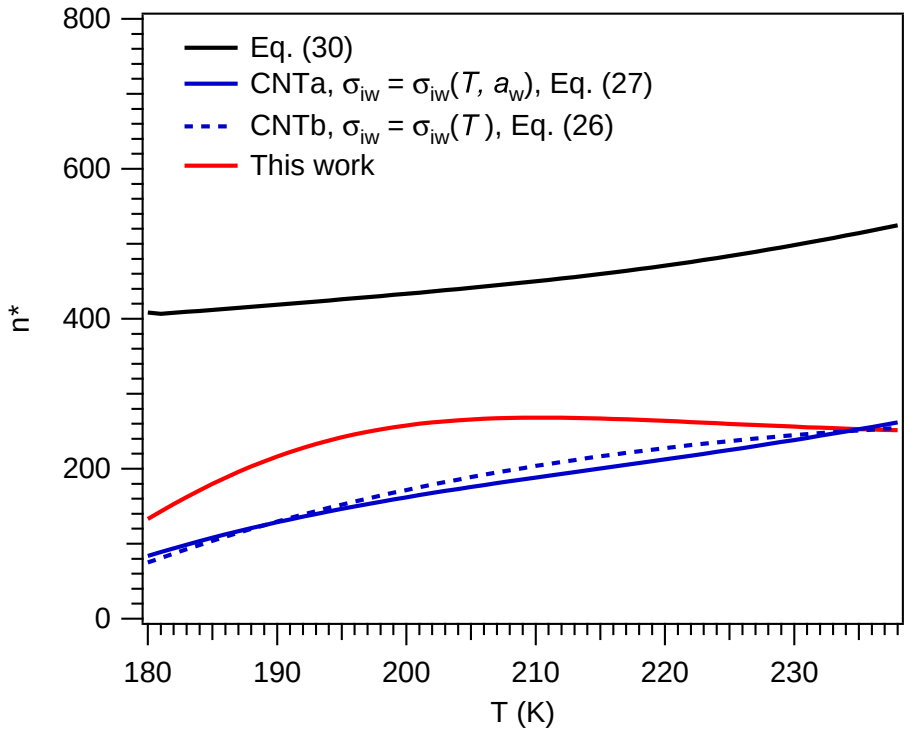

Fig. 3. Critical germ size, n^* calculated at T_f with $D_p = 10\,\mu m$ and $\Delta t = 10\,s$. Results from Eq. (30) were obtained using the correlation of Koop et al. (2000). Lines CNTa and CNTb correspond to classical nucleation theory with and without accounting for a_w effects on σ_{iw}, respectively.

ACPD
14, 1525–1557, 2014

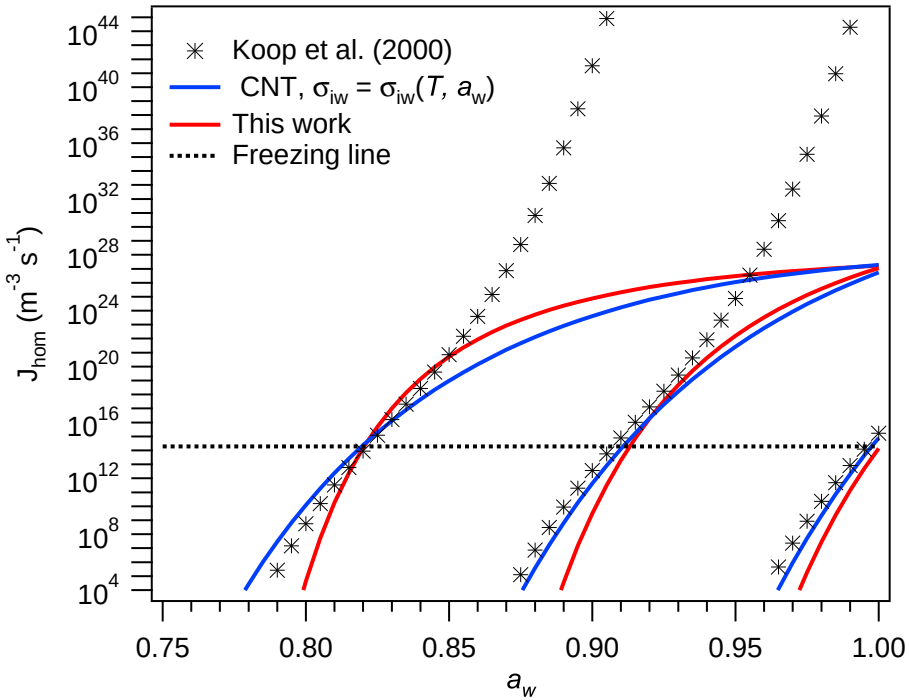

Fig. 4. Homogeneous nucleation rate. The freezing line was calculated using Eq. (28). Lines are grouped by temperature: T = 195, 220 and 236 K, from left to right, respectively.

ACPD
14, 1525–1557, 2014

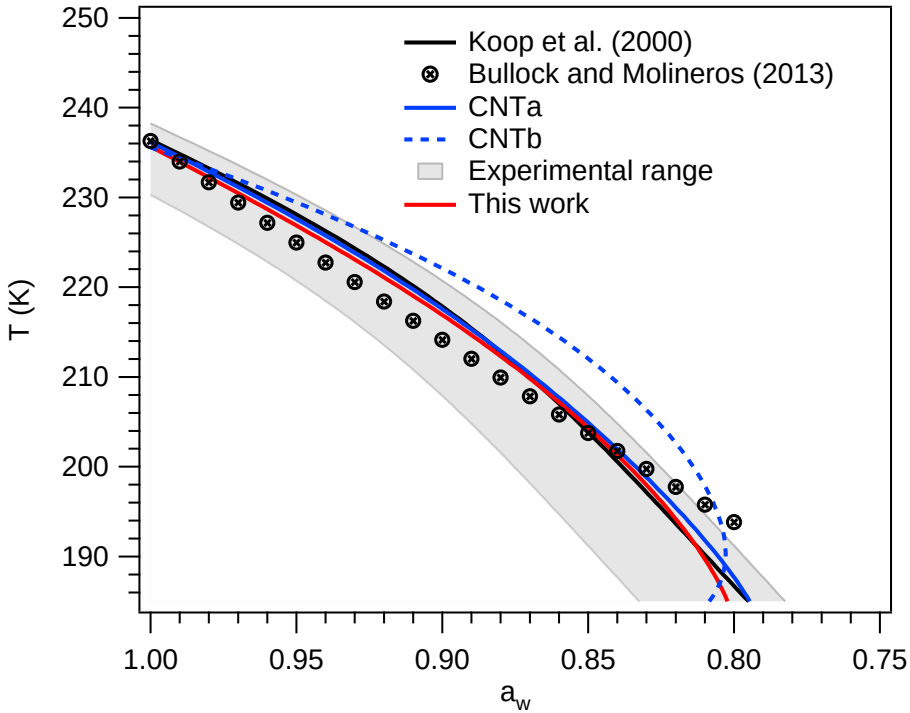

Fig. 5. Freezing temperature for homogeneous nucleation. T_f was found by application of Eq. (28) assuming $D_p = 10\,\mu m$ and $\Delta t = 10$. Lines CNTa and CNTb correspond to classical nucleation theory with and without accounting for a_w effects on σ_{iw}, respectively. Results using the correlation of Bullock and Molinero (2013) are also shown. The experimental range represents $\Delta a_w = 0.313 \pm 0.025$ (Koop and Zobrist, 2009; Alpert et al., 2011).

ACPD
14, 1525–1557, 2014

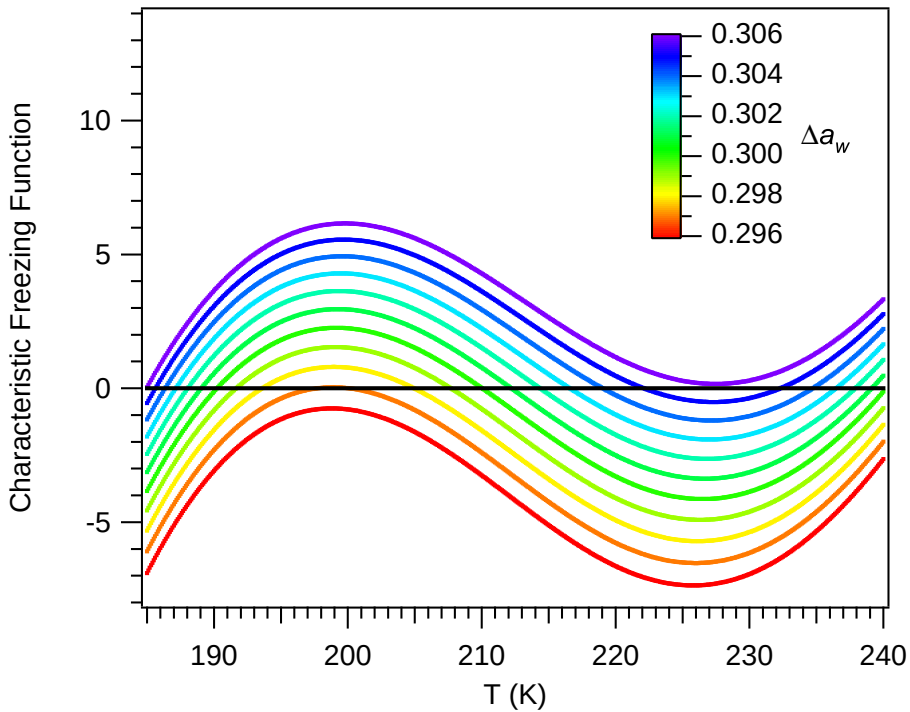

Fig. 6. Characteristic freezing function, Eq. (33), for D_p = 10 µm and Δt = 10 s.

ACPD
14, 1525–1557, 2014